

Effects of urban eutrophication on pelagic habitat capacity in the Southern California Bight

Christina Frieder¹, Fayçal Kessouri¹, Minna Ho^{1,2}, Martha Sutula¹, Daniele Bianchi^{2,3}, James C McWilliams², Curtis Deutsch³, and Evan Howard³

¹Southern California Coastal Water Research Project

²University of California Los Angeles

³Princeton University

March 13, 2023

1 Effects of urban eutrophication on pelagic habitat 2 capacity in the Southern California Bight

3 Christina A. Frieder^{1,*}, Fayçal Kessouri¹, Minna Ho^{1,2}, Martha Sutula¹, Daniele Bianchi²,
4 James C. McWilliams², Curtis Deutsch³, and Evan Howard³

5 ¹Southern California Coastal Water Research Project, Costa Mesa, 92626, USA

6 ²University of California Los Angeles, Los Angeles, 90095, USA

7 ³Princeton University, Princeton, 08544, USA

8 *christinaf@sccwrp.org

9 ABSTRACT

Land-based nutrient inputs to the ocean have been linked to increased coastal productivity, subsurface acidification and O₂ loss, even in upwelling systems like the Southern California Bight. However, whether eutrophication alters the capacity to support key taxa has yet to be evaluated for this region. Here, we assess the impact of land-based nutrient inputs on the availability of aerobic and calcifying habitat for key pelagic taxa using ocean model simulations. We find that acute, lethal conditions are not commonly induced in epipelagic surface waters, but that sublethal, ecologically relevant changes are pervasive. Land-based nutrient inputs reduce the potential aerobic and calcifier habitat during late summer, when viable habitat is at its seasonal minimum. A region of annually recurring habitat compression is found 30 – 90 km from the mainland, southeast of Santa Catalina Island. Here, both aerobic and calcifier habitat is vertically compressed by, on average, 25%, but can be as much as 60%. This effect can be traced to enhanced remineralization of organic matter that originates from the coast. These findings suggest that effects of land-based nutrients are not restricted to chemistry but extend to habitat capacity for multiple taxa of ecological and economic importance. Considerable uncertainty exists, however, in how this habitat compression translates to population-level effects.

11 Introduction

12 Global change is fundamentally restructuring marine ecosystems, shifting distributions, phenologies,
13 and interactions among species. Temperature (T), oxygen (O₂), and carbonate chemistry (e.g., pH, Ω_{Ar})
14 naturally constrain available habitat for marine calcifiers and aerobic animals, but as ocean waters warm,
15 become less oxygenated, and more acidified, these changes are driving habitats beyond the envelope
16 of natural variability, resulting in major changes to species distribution and abundance, and raising the
17 potential for major ecosystem disruptions^{1,2}. While shifts in species abundance or geographic range can
18 be detected in historical data, local human impacts from nitrogen pollution and coastal eutrophication
19 confound the attribution of biological changes to long-term climate trends. Effective coastal ecosystem
20 management in the face of global change requires the means to both: (1) quantify these fundamental
21 changes to species habitats and (2) disentangle the relative roles of climate change, natural and climatic
22 variability, and local anthropogenic pressures in shaping those habitats. Ocean numerical models are
23 routinely used to project the effects of climate change on shifting habitats and species distributions³, but
24 few coastal numerical modeling studies have investigated the potential for local coastal eutrophication to
25 constraint marine calcifier and aerobic habitat⁴. As 50% of the global wastewater receives no treatment
26 before discharging to coastal waters, such studies can help to understand whether local management of
27 coastal eutrophication could meaningfully increase resilience of ecosystems to climate change.

28 Effects of eutrophication on increased primary productivity, enhanced remineralization rates, subsurface
29 O₂ depletion, and acidification are commonly observed within the 100-m isobath, in semi-enclosed
30 seas, and estuaries^{5,6}. However, recent work has revealed that such changes can be meaningful even in
31 upwelling-dominated coastal environments, countering the tenet that low O₂ and Ω_{Ar} that occur along
32 eastern boundary upwelling systems is naturally induced, without direct anthropogenic influence⁷. In
33 the Southern California Bight (SCB), coastal nitrogen export from a human population of 22 million
34 rival natural upwelling in magnitude, roughly doubling available nitrogen⁸. These inputs, which include
35 point and nonpoint source discharges to the ocean from 19 ocean outfalls and 75 rivers, which release,
36 on average, 8 million m³ d⁻¹ of nutrient-enriched water to the ocean⁹, are increasing primary production
37 and subsurface respiration rates along the coast, with corresponding subsurface reductions in O₂ and
38 aragonite saturate state (Ω_{Ar}) that rival or exceed that of global open-ocean O₂ loss and acidification since
39 the pre-industrial period¹⁰.

40 While Kessouri et al.¹⁰ quantified the change in seawater chemistry from anthropogenic nutrient inputs
41 in the Bight, it did not document the potential for biological effects, a fundamental science gap that
42 motivates coastal water quality managers. In the SCB, these changes in seawater chemistry can extend
43 more than 100 km from the coast (~30% of the Bight)¹¹. The region of maximum change occurs in the
44 epipelagic zone, localized between 50 and 200 m water depth. When these declines are superimposed
45 on areas already naturally low in O₂ and Ω_{Ar} , even small changes could be of biogeochemical and
46 ecological significance^{12,13}. The question is whether these subsurface O₂ and acidification changes
47 are occurring at ecologically relevant conditions, resulting in vertical compression of habitat. There are
48 field-based demonstrated consequences of coastal acidification for shell-building zooplankton, in particular
49 pteropods¹⁴. Similarly, O₂ depletion in the ocean can reduce metabolic performance of aerobic taxa¹⁵⁻¹⁷.
50 Most of the literature on hypoxia focuses on acute lethal levels, but sublethal effects, even subtle ones
51 that pose constraints on feeding times, can combine to limit growth or reproduction^{2,18}. Studies in
52 other ecosystems have documented how short-term, low-O₂ events can give rise to immediate habitat
53 compression of sensitive species, increasing susceptibility to overfishing (e.g. of brown shrimp and
54 demersal fishes in the Gulf of Mexico¹⁹ and of artisanal fisheries species in the Sea of Oman²⁰). Even the
55 behavior of smaller vertical-migrating taxa, like copepods, is shaped by seasonal O₂ and temperature²¹.
56 On the longer-term, interactions between temperature and O₂ availability on aerobic metabolism have
57 strong correspondence with faunal diversity, species distributions, predator-prey interactions, and changing
58 biogeographic patterns²²⁻²⁴, and may even result in range shifts^{1,2} and extinction³.

59 In this study, we assess the degree to which modeled O₂ losses and acidification due to land-based nutrient
60 inputs translates to changes in habitat capacity. To accomplish this, we rely on two metrics that define
61 the habitat available for aerobic metabolism and for calcification. Aerobic habitat is determined using
62 the Metabolic Index (Φ), whose trait-based threshold varies across species. Aerobic habitat for northern
63 anchovy, *Engraulis mordax*, is detailed but we also consider how aerobic habitat is modified across the
64 full range of metabolic traits. Calcifying habitat is based on the saturation state of aragonite (Ω_{Ar}), whose
65 thresholds also vary among species. We evaluate calcifier habitat capacity as the thickness of the water
66 column where $\Omega_{Ar} \geq 1.4$, but we also consider the sensitivity of our results to other values of Ω_{Ar} . Our
67 study objectives are threefold. First, we evaluate temporal and spatial patterns in aerobic and calcifier
68 habitat capacity metrics in the SCB with output from a 20-year numerical ocean model hindcast. Second,
69 we test how anthropogenic nutrient inputs from land-based sources alter the vertical thickness of the habitat
70 capacity metrics. We rely on two model scenarios, the first includes natural oceanic cycles of nutrients, O₂
71 and carbon, to which rising global CO₂ emissions have been imposed (referred to hereafter as 'CTRL'),
72 and the second includes both natural oceanic cycles of nutrients with inputs from terrestrial sources, 98%

73 of which are anthropogenic and 95% of which are point source in origin (referred to hereafter as ‘ANTH’)⁹.
74 Third, we confirm the mechanisms by which anthropogenic nutrients contribute to the observed changes
75 in vertical habitat capacity by analyzing changes in the biogeochemical rate processes that contribute to
76 the O₂ and carbon cycle.

77 Results

78 For both habitat capacity metrics, there are consistent Bight-wide spatial and temporal patterns (Fig. 1),
79 with calcifier habitat thickness greater than anchovy aerobic habitat thickness. Calcifier habitat thickness
80 ranges from, on average, 80 to 130 m. Anchovy aerobic habitat thickness ranges, on average, from 50 to
81 100 m. Both habitat thickness metrics are most restricted within the Santa Barbara Channel and around
82 San Nicolas Island. Increases generally occur along north-to-south and onshore-to-offshore gradients.

83 The dominant temporal scales of calcifier and anchovy aerobic habitat capacity are inter-annual and
84 seasonal (Fig. 1). The temporal mean of total calcifier and anchovy aerobic habitat volumes are 8.2 and
85 $5.4 \times 10^3 \text{ km}^3$, respectively, summed across the model domain. Among years, total volume for each
86 metric can vary approximately 2-fold. In 2011, calcifier and anchovy aerobic habitat volumes were most
87 restricted at 4.2 and $3.6 \times 10^3 \text{ km}^3$; in 1998, habitat volumes were most expansive at 10.2 and 6.2×10^3
88 km^3 , respectively. Seasonal variability also drives approximately 2-fold changes in habitat volumes. An
89 evaluation of the annually detrended time series for both metrics shows that total habitat volumes are
90 greatest during winter months and contract during summer, with the least amount of total habitat available
91 during July and August (Fig. 1D-E). Since anchovy aerobic habitat is constrained by both temperature and
92 O₂, attribution analysis reveals that O₂ is the primary contributor to seasonal trends in total habitat volume,
93 and that seasonal changes in temperature counteract that of O₂ (Fig. S1).

94 There is not a consistent tendency for land-based nutrient inputs to result in consistent or persistent
95 Bight-wide calcifier and aerobic habitat capacity gains or losses (Fig. S2). The relative, Bight-wide
96 differences in total habitat volume vary by $\pm 5\%$ for most of the period simulated. However, at any
97 grid cell location, the difference in calcifier habitat thickness between ANTH and CTRL can range from
98 -34 to $+45\%$, and that for anchovy aerobic habitat ranges from -43 to $+80\%$ (1st and 99th percentiles,
99 respectively).

100 A spatial perspective of the change in calcifier and anchovy aerobic habitat thickness reveals a region
101 of habitat loss that is expressed southeast of Santa Catalina Island (Fig. S2). This region of habitat loss
102 is a seasonal phenomenon. In seven of the nine years simulated, there is a compression event lasting
103 approximately 2.5 months that occurs in the late summer to early fall (Fig. 2c-d), a time period when
104 calcifier and anchovy aerobic habitat thickness are already seasonally compressed (Fig. 1d-e). Averaging
105 across these seven compression events, the total spatial area experiencing recurrent calcifier habitat change
106 is $2,364 \text{ km}^2$ (assessed as the total spatial area where the change in calcifier habitat thickness $\leq -20\%$; Fig.
107 2a) The equivalent total spatial area experiencing recurrent anchovy aerobic habitat change is $1,909 \text{ km}^2$
108 (Fig. 2b). Despite the temporal overlap in natural seasonal and eutrophication-driven compression, there
109 is spatial mismatch between the regions undergoing maximum habitat compression due to eutrophication
110 with those that are naturally most restricted from broad-scale oceanographic patterns (e.g., Santa Barbara
111 Channel; Fig. 1a-b).

112 Anchovy represent one ecophysiotype in a range of metabolic trait possibilities. Quantifying aerobic
113 habitat change across the full range of Metabolic Index trait combinations (E_o and A_o/Φ_{CRIT}) demonstrates
114 that not all ecophysiotypes are subject to aerobic habitat loss (Fig. 33A). Ecophysiotypes with higher

115 hypoxia tolerance (A_o/Φ_{CRIT}) gain aerobic habitat volume; while those with lower hypoxia tolerance,
116 including anchovy, lose aerobic habitat volume. Taking a species-weighted distribution of metabolic trait
117 possibilities, approximately two-thirds of species are losing aerobic habitat volume, and the modeled
118 losses can be up to three times greater than the gains (Fig. 3b). Of those subjected to aerobic habitat loss,
119 70% of species are subject to more habitat loss than northern anchovy (Table S1). These species that are
120 gaining aerobic habitat volume have higher hypoxia tolerance at any given temperature sensitivity (E_o ;
121 Fig. 3a), with the biggest gain in aerobic habitat volume available for Humboldt squid, *Dosidicus gigas*
122 (Table S1).

123 The spatial and vertical distribution of greatest O_2 change is occurring between approximately 40 and
124 100 km from the coast and between 50 and 150 meters or more below the surface (Fig. 4b). The same
125 pattern is observed for acidification, assessed as the difference in Ω_{Ar} between the two scenarios (Fig.
126 4b). The lower limit of anchovy aerobic habitat coincides in space with the region of maximum O_2 loss.
127 In the CTRL scenario, the anchovy aerobic habitat limit is at 80 m in the offshore region of maximum
128 O_2 loss (60 km from the coast), and shoals to 60 m in the ANTH scenario. In contrast, the lower limit
129 for calcifier habitat thickness is deeper than the vertical region undergoing maximum acidification. Still,
130 calcifier habitat thickness shoals from approximately 115 m in the CTRL scenario to 87 m in the ANTH
131 scenario. Because both subsurface acidification and O_2 loss occur across a broad depth range, our results
132 are largely insensitive to which value of Ω_{Ar} is used to define optimal calcifier habitat (Fig. S3). Similarly,
133 loss of O_2 is occurring across a broad depth range (Fig. S4). Notably, these changes to habitat capacity in
134 the epipelagic are largely limited to sublethal effects as conditions that trigger acute lethal effects occur
135 deeper in the water column. Conditions where Ω_{Ar} are less than 1 occur, on average, deeper than 200
136 m water depth (Fig. S3). Similarly, acute lethal O_2 conditions ($\Phi = 1$) for northern anchovy occurs, on
137 average, much deeper than 300 m water depth, well below the typically observed vertical distributions of
138 anchovy and other pelagic fishes.

139 Of the biogeochemical rate processes contributing to habitat change within the region of 20% habitat
140 compression, remineralization rates are exhibiting the greatest absolute change due to land-based nutrient
141 inputs (Fig. 5). For the carbon cycle, remineralization rates increase from 4.26 ± 0.12 to 4.50 ± 0.12
142 $\text{mmol DIC m}^{-3} \text{d}^{-1}$ from the CTRL to the ANTH scenario (mean ± 1 SE; $N = 104$ months). The increase
143 in DIC from land-based nutrient inputs at the core of habitat compression drives the modeled decrease
144 in Ω_{Ar} . Small changes in alkalinity ($< 5 \text{ mmol m}^{-3}$) counteract the effects due to DIC (Fig. S5). For the
145 O_2 cycle, remineralization rates are also exhibiting the greatest change due to land-based nutrient inputs,
146 changing from -5.44 ± 0.15 to $-5.75 \pm 0.15 \text{ mmol O}_2 \text{ m}^{-3} \text{d}^{-1}$ from CTRL to ANTH (mean ± 1 SE; N
147 $= 104$ months).

148 Discussion

149 Here, we demonstrate that eutrophication effects of land-based nutrient export to the Southern California
150 Bight are not restricted to changes in seawater acidification and O_2 loss¹¹, but also extend to the potential
151 for widespread effects on calcifier and aerobic habitat capacity. The seawater chemistry changes that
152 occur in the epipelagic are not at conditions that elicit acute, lethal effects. However, the habitat capacity
153 metrics used here are sensitive to eutrophication, changes recurring annually despite large, natural seasonal
154 and interannual cycles (Fig. 1). During the late summer, subsurface acidification and O_2 loss routinely
155 compress aerobic and calcifier habitat capacity (Fig. 2), at a time period when habitat capacity is already
156 seasonally compressed (Fig. 1). Modeled habitat compression is most pronounced where excess nutrients
157 and organic matter, which originate at the coast, are received and entrained within offshore eddies¹¹. Since

158 seawater chemistry changes due to enhanced remineralization are occurring across a large depth range,
159 patterns in habitat compression are largely insensitive to the value of Ω_{Ar} used to define the calcifier
160 habitat capacity metric (Fig. S3). Similarly, while we evaluate aerobic habitat capacity for northern
161 anchovy, we confirm that this pattern is consistent among two thirds of ecophysiotypes (although at
162 differing magnitudes of loss), and that those species gaining aerobic habitat volume have higher active
163 tolerances to low O_2 (Fig. 3).

164 There is field-based evidence that the vertical structure of both Ω_{Ar} and O_2 have implications for a variety
165 of pelagic taxa. For example, across frontal gradients in the California Current System where Ω_{Ar} between
166 1.0 and 1.4 can shoal by 100+ m on the scale of tens of kms, there are concurrent reductions in pteropod
167 abundance accompanied by elevated shell dissolution²⁵. From onshore-to-offshore gradients, more severe
168 pteropod shell dissolution and thinner shells occur close to the coast, particularly where upwelling is more
169 intense^{26,27}. The predicted habitat compression described here coincides with the natural seasonal cycle
170 of limited habitat availability. Multiple species of pteropods, including *Limacina helicina*, are present
171 year-round in the SCB (K. McLaughlin, pers. comm.). While limited baseline information on pteropod life
172 history characteristics exist for the Southern California Bight²⁸, studies suggested that spring (April-May)
173 and fall (September- October) are periods when early life stage cohorts are most vulnerable to changing
174 ocean conditions²⁹⁻³¹.

175 Ocean O_2 depletion adversely impacts marine species, assemblages, and even fisheries³². Long-term
176 deoxygenation trends play a role in, for example, declines in abundance of mesopelagic fishes³³ and
177 shifts in zooplankton and small nekton diel migration depth³⁴. Interactive effects of sub-optimal O_2 and
178 temperature are becoming increasingly considered¹³. Sub-optimal O_2 stress depends on the O_2 supply
179 relative to metabolic demand, and water temperature controls both chemical (O_2 solubility, diffusivity) and
180 physiological processes (metabolic demand, ventilations rates) affecting this balance for marine ectotherms.
181 We use the mechanistic framework of the Metabolic Index²² to incorporate these dependencies into the
182 index of aerobic habitat capacity. Specific to our focal taxa, northern anchovy have seasonal to interdecadal
183 redistributions that correlate with aerobic habitat capacity. For example, anchovy migrate offshore during
184 peak upwelling seasons^{35,36}, when nearshore aerobic habitat availability is lowest, even though their food
185 supply is generally higher closer to the coast¹. Further, the southern biogeographic limit of this species
186 is coincident with the aerobic habitat capacity threshold implied by their oscillations in time within the
187 SCB, and vice versa¹. While reductions in this index are associated with species-specific consequences
188 of deoxygenation at the regional scale, it remains unclear how the spatial and seasonal extent of the O_2
189 reduction identified here might translate to disruptions across species of varying phenologies, mobility, and
190 ecological niches. The same can be said for the population-level consequences of subsurface acidification.

191
192 We evaluate O_2 loss and acidification effects on habitat capacity separately, as the combined effects of these
193 stressors on biological responses are insufficiently understood⁴. However, studies suggest that exposure to
194 suboptimal ranges of acidification, O_2 , and temperature can make marine organisms more sensitive to O_2
195 loss³⁷ or less resilient to acidification³⁸. In this model domain, there is strong covariance between calcifier
196 and aerobic habitat thickness (Pearson correlation coefficient = 0.79), linked to eutrophication effects on
197 water-column remineralization, such that aerobic and calcifier habitat compress at the same time. Thus,
198 predicted effects on habitat capacity for marine species may be underestimated⁴. The Metabolic Index
199 framework does incorporate the combined effects of temperature and O_2 . Biological sensitivities to all
200 three variables – temperature, O_2 , and carbonate system state – could potentially be merged through a
201 fundamental physiological trait such as aerobic scope (i.e., a proxy for the surplus energy available for

202 growth, reproduction, predator avoidance, etc.).

203 While we emphasize subsurface losses in habitat capacity, anthropogenic nutrient loads can also enhance
204 productivity and food supply in coastal ecosystems, thereby potentially reducing the negative consequences
205 of suboptimal O₂ and acidification^{39,40}. As an example, total fisheries landings can remain high even if
206 demersal species in O₂-depleted areas decline, because nutrients can stimulate prey production in other
207 well-mixed parts of a system^{39,41}. Abundant prey can improve stress tolerance of organisms⁴². However,
208 system-wide compensation through enhanced productivity will have limits as the volume of O₂-depleted
209 waters expand⁴³. The catch per unit effort for selected demersal fish species along the U.S. West Coast
210 is positively related to near-bottom O₂ concentrations, with the catch per unit effort decreasing more
211 significantly as O₂ concentrations decrease⁴⁴. In the Humboldt Current, it is suggested that low O₂ near
212 the coast results in a highly efficient trophic transfer and a dense anchovy population⁴⁵, which is beneficial
213 for fishing activities. During these conditions, species that are less tolerant to low O₂, like sardine and jack
214 mackerel, are restricted to offshore, well-oxygenated waters^{46,47}.

215 Global climate change will further exacerbate habitat loss resulting from land-based nutrient inputs¹⁰.
216 Strengthened stratification, from increased surface water temperatures as the global climate warms, is
217 sufficient to worsen subsurface O₂ and acidification where it currently exists and may instigate habitat
218 loss elsewhere⁴⁸. Warming and O₂ loss by 2100 are projected to result in complete loss of aerobic
219 habitat for northern anchovy – and thus likely extirpation – from the southern California Current System
220 (CCS)¹. Further, the interplay of anthropogenic nutrient export and stratification where they occur could
221 accelerate the timeline of habitat compression and potential extirpation. In this study, O₂ loss in the core
222 of habitat compression exceeds 30 μmol kg⁻¹ (Fig. 4c). This is 1.5 times the scale of decadal O₂ loss
223 in the southern CCS which may be occurring at around 20 μmol kg⁻¹ decade⁻¹⁴⁹. Acidification in the
224 same eutrophication-induced core exceeds –0.3 units for Ω_{Ar}, and this is three times the decadal trend of
225 approximately –0.1 decade⁻¹^{50,51}.

226 To conclude, we assess change in habitat capacity for pelagic calcifying and aerobic taxa due to eutroph-
227 ication effects on subsurface acidification and O₂ loss from land-based nutrients. Our findings suggest
228 that effects of land-based nutrients are not restricted to chemistry. Changes to habitat capacity defined
229 by sublethal, ecologically relevant thresholds were pervasive during late summer, when habitat capacity
230 is at its seasonal minimum. Despite the theoretical, experimental, and field evidence that identify the
231 importance of the vertical structure of both carbonate chemistry and O₂ for marine pelagic communities,
232 whether the modeled habitat compression shown here translate to population-level effects is uncertain.
233 Actions to increase this certainty can include the expansion of a habitat capacity metric that includes the
234 interactive effects of acidification and O₂ loss, consideration of how these outcomes interplay with food
235 availability, and investigation into the scales at which spatial and temporal changes in habitat capacity
236 translate to population-level effects. All of which can be bolstered by robust, region-wide modeling,
237 experimental, and field programs.

238 **Methods**

239 To assess whether modeled effects of land-based nutrient inputs on Bight-wide subsurface O₂ loss and
240 acidification are biologically relevant, we employed two metrics for habitat capacity, which we adapted
241 for this purpose. One incorporates temperature-dependent environmental O₂ as a predictor of habitat
242 capacity for aerobic metabolism and the other incorporates carbonate chemistry as a predictor of habitat
243 capacity for aragonite production by calcifiers. The premise of our approach is that these metrics provide
244 information on the capacity of a specified location to provide habitat conditions that are sufficient for key

245 processes for a species, or group of species, based on either empirical or mechanistic relationships of
246 organismal performance with the environmental condition(s) of interest. The habitat capacity metrics are
247 applied to model outputs from scenarios with and without land-based nutrient inputs in order to perform a
248 difference assessment. Each metric is presented as the volume or vertical thickness of water-column as
249 spatial gradients in both O₂ and carbonate chemistry are greatest in the vertical dimension.

250 Since modeled effects of subsurface O₂ loss and acidification due to anthropogenic nutrient inputs are
251 shown to be localized between 50 and 200 m¹¹, we focus our analysis on pelagic taxa. Because literature
252 is limited on the interactive effects of O₂ and carbonate chemistry in these environments, we adapt two
253 separate metrics to evaluate the changes in O₂ versus the changes in carbonate chemistry with an emphasis
254 on aerobic taxa and calcifiers, accordingly.

255 For the effects of subsurface acidification on calcifier habitat capacity, we calculate the vertical thickness
256 of optimal aragonite saturation state (Ω_{Ar}) conditions. A value of Ω_{Ar} of 1.4 is used to define the condition
257 below which sublethal organismal responses have been documented to commonly occur^{14,52,53}. One of the
258 primary lines of evidence for this choice is derived from a synthesis of documented effects on pteropods¹⁴,
259 in which Ω_{Ar} thresholds for a range of sublethal to lethal responses were identified and confidence in
260 thresholds were judged with expert consensus. Pteropods are ubiquitous, holoplanktonic calcifiers that
261 have a well-documented, specific sensitivity to ocean acidification. These calcifiers efficiently transfer
262 energy from phytoplankton to higher trophic levels^{54,55}, and as such serve as an important prey group for
263 ecologically and economically important fishes, bird, and whale diets^{56–58}. Bednaršek et al.¹⁴ identified
264 that Ω_{Ar} from 1.5 – 0.9 provides a risk range from mild dissolution to lethal impacts. Our selected value
265 of Ω_{Ar} of 1.4 represents a value within observational analytical precision (± 0.2 ⁵⁹) of thresholds where
266 sublethal effects on calcification, growth, and severe dissolution are documented to occur, while a value
267 of 1.0 roughly equates to lethal effects (0.9 to 0.95¹⁴). In the epipelagic (0-200 m), conditions below
268 saturation have not been common in the modern ocean but are predicted to emerge as soon as the 2030's
269 and 2040's⁶⁰. Importantly, we perform an analysis of the sensitivity of our findings to the choice of Ω_{Ar}
270 along this range of 1.0 to 1.4 and find the results to be largely sensitive within this range (see Analytical
271 Approach for further details).

272 For the effects of subsurface O₂ loss on aerobic habitat capacity, we calculate the vertical thickness of
273 the water column that has sufficient O₂ to provide ecological support for northern anchovy (*Engraulis*
274 *mordax*). Northern anchovy is also holoplanktonic with greatest abundance observed in the upper 100 m³⁵.
275 Defining sufficient O₂ for ecological support relies on the mechanistic framework of the Metabolic Index
276 (Φ ^{22,23}). Φ is defined as the ratio of O₂ supply to resting demand. We can calculate the habitat thickness
277 for which $\Phi/\Phi_{CRIT} \geq 1$, a value below which demarcates environment in which anchovy can sustain
278 resting but not active energetic demands, thus limiting population persistence. For northern anchovy,
279 metabolic traits have been inferred from observational datasets associated with climatological O₂ and
280 temperature conditions¹. While we use metabolic traits for northern anchovy as our primary analysis, we
281 consider how modeled O₂ loss interacts with the full range of metabolic trait combinations. Similarly, we
282 evaluate a lethal threshold for northern anchovy, where $\Phi = 1$ and O₂ supply is insufficient to meet O₂
283 demand. This latter analysis converts the reported active hypoxia threshold (A_o/Φ_{CRIT}) to the value at rest
284 (A_o) using $\Phi_{CRIT} = 3.5$, the mean value across marine organisms (Deutsch et al. 2020); some species have
285 Φ_{CRIT} as low as 1.5, in which case the lethal thresholds could occur at proportionately higher values of O₂
286 and thus at shallower depths.

287 We utilize biogeochemical output from the Regional Ocean Modeling System, ROMS⁶¹, coupled to the
288 Biogeochemical Elemental Cycling model, BEC⁶², which has been adapted for the CCS^{63,64}. BEC is a

289 multi-element (C, N, P, O, Fe, and Si) and multi-plankton model that includes three explicit phytoplankton
 290 functional groups (picoplankton, silicifying diatoms, and N-fixing diazotrophs), one zooplankton group,
 291 and dissolved and sinking organic detritus. Remineralization of sinking organic material follows the
 292 multi-phase mineral ballast parameterization of Armstrong et al.⁶⁵, and sedimentary processes have also
 293 been expanded. Particulate organic matter reaching the sediment is accumulated and remineralized with a
 294 time scale of 330 days, to provide a buffer between particle deposition and nutrient release. The ecosystem
 295 is linked to a carbon system module that tracks dissolved inorganic carbon and alkalinity, and an air–sea
 296 gas exchange module based on the formulation of Wanninkhof⁶⁶.

297 The SCB model domain, which extends from Tijuana Mexico to Pismo Beach (U.S. Central California
 298 coast) and about 200-km offshore, is part of a nested configuration. Model nests scale from a 4-km
 299 horizontal resolution configuration spanning the entire CCS, to a 1-km resolution grid covering much of
 300 the California coast (latitude < 40.25°N), to a 0.3-km grid in the SCB, where our investigations of local
 301 anthropogenic inputs were focused^{10,67}. This grid, shown in Fig. 1a, is composed of 1,400 × 600 grid
 302 points, with 60 σ -coordinate vertical levels using the stretching function described in Shchepetkin and
 303 McWilliams⁶¹. The model is run with a time step of 30 s, and outputs are saved as 1-day averages. More
 304 information on the model setup and forcing is provided in other works^{63,64,67}.

305 ROMS-BEC has been validated for atmospheric forcing, physics, and biogeochemistry including O₂,
 306 carbonate saturation state, primary productivity, and hydrographic parameters at a West Coast-wide scale⁶³
 307 and, within the SCB, at scales at which anthropogenic nutrients influence coastal eutrophication⁶⁷.

308 We rely on two model scenarios. The first includes only natural oceanic cycles of nutrients (CTRL) and
 309 thus represents only natural ocean cycles of nutrient, carbon, and O₂, with the effects of global CO₂
 310 superimposed. The second represents these same CTRL base conditions, to which inputs from terrestrial
 311 sources are added, 98% of which are anthropogenic and 95% of which are point source in origin (ANTH)⁹.
 312 Model simulations that include terrestrial inputs were forced with a monthly time series of spatially explicit
 313 inputs, including freshwater flow, nitrogen, phosphorus, silica, iron, and organic carbon representing
 314 natural and anthropogenic sources⁹. These data include POTW ocean outfalls and riverine discharges
 315 (1997–2017) and spatially explicit modeled estimates of atmospheric deposition. POTW effluent data
 316 were compiled from permit monitoring databases and communication with sanitary agencies. Monthly
 317 time series of surface water runoff from 75 rivers are derived from model simulations and monitoring
 318 data⁹. The CTRL simulation covers the time periods of 02/1997 – 01/2001 and 08/2012 – 11/2017. The
 319 ANTH simulation covers the time period of 02/1997 – 11/2017.

320 Aragonite saturation state was computed with the CO2SYS algorithms^{68,69} using daily averages of model
 321 output fields of dissolved inorganic carbon (DIC), total alkalinity (TA), temperature, salinity, and pressure.
 322 Calcifier habitat thickness was calculated as the thickness of the water column for each grid cell that was
 323 \geq optimal Ω_{Ar} (1.4) for pteropods.

324 The ecological Metabolic Index (Φ/Φ_{CRIT}) was computed from daily averages of model output fields of
 325 O₂ and temperature.

$$\frac{\Phi}{\Phi_{CRIT}} = \frac{A_o}{\Phi_{CRIT}} \times \frac{pO_2}{\exp(-E_o/k_B(1/T - 1/T_{ref}))} \quad (1)$$

326 The metabolic traits of northern anchovy are $A_o/\Phi_{CRIT} = 5.4 \text{ atm}^{-1}$ (equivalent to an active hypoxia
 327 threshold of $pO_2 = 0.185 \text{ atm}$ at 15°C) and $E_o = 0.4 \text{ eV}$ (the net temperature sensitivity of O₂ supply

328 and demand)¹. pO_2 is the environmental partial pressure of O_2 and T is temperature (in K). k_B is the
329 Boltzmann constant and T_{ref} is the reference temperature (here, 288.15 K). Aerobic habitat thickness was
330 calculated as the thickness of the water column where $\Phi/\Phi_{CRIT} \geq 1$.

331 Spatial and temporal patterns in calcifier and aerobic habitat thickness were evaluated with the ANTH
332 simulation to identify the dominant spatial and temporal scales of variability in each. Total calcifier and
333 aerobic habitat for the model domain was summed across all grid cells as the habitat thickness within a
334 grid cell multiplied by the area of that grid cell.

335 To then evaluate how anthropogenic nutrient inputs alter calcifier and aerobic habitat thickness, we
336 perform a difference assessment (ANTH-CTRL) where positive (negative) values represent an expansion
337 (contraction) of habitat thickness attributable to anthropogenic nutrient inputs included in the ANTH
338 scenario only. We focus further analyses in regions where differences in habitat thickness exceed \pm
339 20%. To test the sensitivity of calcifier habitat capacity to the value of Ω_{Ar} , we evaluate habitat thickness
340 for $\Omega_{Ar} \geq 1.0 - 2.5$. We also calculate the change in water-column thickness for a range of $[O_2]$ from
341 60 – 200+ $mmol\ m^{-3}$. Since northern anchovy, our species of focus for aerobic habitat, is just one
342 ecophysiotype among a range of possibilities, we evaluate the change in aerobic habitat volume across the
343 full combination of metabolic trait possibilities (A_o/Φ_{CRIT} and E_o) and estimate the fraction of species
344 undergoing trait-weighted volume changes with a probability distribution of empirical traits (derived by
345 Penn and Deutsch³).

346 For regions undergoing more than a $\pm 20\%$ change in habitat thickness, we evaluate the difference in the
347 biogeochemical rate processes from each scenario (detailed methods provided in Deutsch et al.⁶³ and
348 Kessouri et al.¹¹). Biogeochemical rate processes that influence the O_2 cycle include surface air-sea flux,
349 photosynthesis, non-grazing mortality, grazing mortality, water-column remineralization, sediment-water
350 flux, NH_4 oxidation, and nitrification (Eq. A9 in Deutsch et al.⁶³). Biogeochemical rate processes that
351 influence dissolved inorganic carbon include air-sea flux, photosynthesis, $CaCO_3$ production, non-grazing
352 mortality, grazing mortality, and water-column and sediment remineralization (Eq. A11 in Deutsch et
353 al.⁶³). We perform a difference assessment from the monthly averages for the sum of the biogeochemical
354 process terms. This analysis is focused between 70 and 140-m water depth to align with the depth range
355 where habitat thickness is affected.

356 References

- 357 1. Howard, E. M. *et al.* Climate-driven aerobic habitat loss in the California Current System. *Sci. Adv.* **6**,
358 eaay3188 (2020).
- 359 2. Pinsky, M. L., Selden, R. L. & Kitchel, Z. J. Climate-driven shifts in marine species ranges: Scaling
360 from organisms to communities. *Annu. Rev. Mar. Sci.* **12**, 153–179 (2020).
- 361 3. Penn, J. L. & Deutsch, C. Avoiding ocean mass extinction from climate warming. *Science* **376**,
362 524–526 (2022).
- 363 4. Bednaršek, N., Pelletier, G., Ahmed, A. & Feely, R. A. Chemical exposure due to anthropogenic
364 ocean acidification increases risks for estuarine calcifiers in the salish sea: Biogeochemical model
365 scenarios. *Front. Mar. Sci.* **7**, 580 (2020).
- 366 5. Rabalais, N. Eutrophication. In Robinson, A. R. & Brink, K. H. (eds.) *The Global Coastal Ocean: Mul-*
367 *tiscale Interdisciplinary Processes*, vol. 13, chap. 21, 821–866 (Harvard University Press, Cambridge,
368 Massachusetts and London, 2005).

- 369 **6.** Rabalais, N. N., Turner, R. E., Díaz, R. J. & Justić, D. Global change and eutrophication of coastal
370 waters. *ICES J. Mar. Sci.* **66**, 1528–1537, DOI: [10.1093/icesjms/fsp047](https://doi.org/10.1093/icesjms/fsp047) (2009).
- 371 **7.** Fennel, K. & Testa, J. M. Biogeochemical controls on coastal hypoxia. *Annu. Rev. Mar. Sci.* **11**,
372 105–130 (2019).
- 373 **8.** Howard, M. D. *et al.* Anthropogenic nutrient sources rival natural sources on small scales in the
374 coastal waters of the Southern California Bight. *Limnol. Oceanogr.* **59**, 285–297 (2014).
- 375 **9.** Sutula, M. *et al.* A baseline of terrestrial freshwater and nitrogen fluxes to the Southern California
376 Bight, USA. *Mar. Pollut. Bull.* **170**, 112669, DOI: <https://doi.org/10.1016/j.marpolbul.2021.112669>
377 (2021).
- 378 **10.** Kessouri, F. *et al.* Coastal eutrophication drives acidification, oxygen loss, and ecosystem change in a
379 major oceanic upwelling system. *Proc. Natl. Acad. Sci.* **118**, e2018856118 (2021).
- 380 **11.** Kessouri, F. Large-scale response to urban eutrophication in the southern California Current System.
381 (Submitted).
- 382 **12.** Levin, L. A. Manifestation, drivers, and emergence of open ocean deoxygenation. *Annu. Rev. Mar.*
383 *Sci.* **10**, 229–260, DOI: [10.1146/annurev-marine-121916-063359](https://doi.org/10.1146/annurev-marine-121916-063359) (2018).
- 384 **13.** Roman, M. R., Brandt, S. B., Houde, E. D. & Pierson, J. J. Interactive effects of hypoxia and
385 temperature on coastal pelagic zooplankton and fish. *Front. Mar. Sci.* **6**, 139 (2019).
- 386 **14.** Bednaršek, N. *et al.* Systematic review and meta-analysis toward synthesis of thresholds of ocean
387 acidification impacts on calcifying pteropods and interactions with warming. *Front. Mar. Sci.* **6**, 227
388 (2019).
- 389 **15.** Fry, F. The effect of environmental factors on the physiology of fish. In Hoar, W. & Randall, D. (eds.)
390 *Environmental Relations and Behavior*, vol. 6 of *Fish Physiology*, 1–98, DOI: [https://doi.org/10.1016/](https://doi.org/10.1016/S1546-5098(08)60146-6)
391 [S1546-5098\(08\)60146-6](https://doi.org/10.1016/S1546-5098(08)60146-6) (Academic Press, 1971).
- 392 **16.** Pörtner, H. O. & Knust, R. Climate change affects marine fishes through the oxygen limitation of
393 thermal tolerance. *Science* **315**, 95–97 (2007).
- 394 **17.** Seibel, B. A. Critical oxygen levels and metabolic suppression in oceanic oxygen minimum zones. *J.*
395 *Exp. Biol.* **214**, 326–336, DOI: [10.1242/jeb.049171](https://doi.org/10.1242/jeb.049171) (2011).
- 396 **18.** Gunderson, A. R. & Leal, M. A conceptual framework for understanding thermal constraints on
397 ectotherm activity with implications for predicting responses to global change. *Ecol. Lett.* **19**, 111–120
398 (2016).
- 399 **19.** Craig, J. K. Aggregation on the edge: effects of hypoxia avoidance on the spatial distribution of brown
400 shrimp and demersal fishes in the northern Gulf of Mexico. *Mar. Ecol. Prog. Ser.* **445**, 75–95 (2012).
- 401 **20.** Piontkovski, S. A. & Al-Oufi, H. S. Oxygen minimum zone and fish landings along the Omani shelf.
402 *J. Fish. Aquatic Sci.* **9**, 294 (2014).
- 403 **21.** Pierson, J. J., Slater, W.-C. L., Elliott, D. & Roman, M. R. Synergistic effects of seasonal deoxygena-
404 tion and temperature truncate copepod vertical migration and distribution. *Mar. Ecol. Prog. Ser.* **575**,
405 57–68 (2017).
- 406 **22.** Deutsch, C., Ferrel, A., Seibel, B., Pörtner, H.-O. & Huey, R. B. Climate change tightens a metabolic
407 constraint on marine habitats. *Science* **348**, 1132–1135 (2015).
- 408 **23.** Deutsch, C., Penn, J. L. & Seibel, B. Metabolic trait diversity shapes marine biogeography. *Nature*
409 **585**, 557–562 (2020).

- 410 **24.** Seibel, B. A. Cephalopod susceptibility to asphyxiation via ocean incalcescence, deoxygenation, and
411 acidification. *Physiology* **31**, 418–429 (2016).
- 412 **25.** Bednaršek, N. & Ohman, M. Changes in pteropod distributions and shell dissolution across a frontal
413 system in the California Current System. *Mar. Ecol. Prog. Ser.* **523**, 93–103 (2015).
- 414 **26.** Feely, R. A. *et al.* Chemical and biological impacts of ocean acidification along the west coast of
415 North America. *Estuarine, Coast. Shelf Sci.* **183**, 260–270 (2016).
- 416 **27.** Mekkes, L. *et al.* Pteropods make thinner shells in the upwelling region of the California Current
417 Ecosystem. *Sci. Reports* **11**, 1731 (2021).
- 418 **28.** Manno, C. *et al.* Shelled pteropods in peril: assessing vulnerability in a high CO₂ ocean. *Earth-Science*
419 *Rev.* **169**, 132–145 (2017).
- 420 **29.** Gannefors, C. *et al.* The arctic sea butterfly *Limacina helicina*: lipids and life strategy. *Mar. Biol.*
421 **147**, 169–177 (2005).
- 422 **30.** Wang, K. *The life cycle of the pteropod Limacina helicina in Rivers Inlet (British Columbia, Canada).*
423 Ph.D. thesis, University of British Columbia (2014).
- 424 **31.** Wang, K., Hunt, B. P., Liang, C., Pauly, D. & Pakhomov, E. A. Reassessment of the life cycle of the
425 pteropod *Limacina helicina* from a high resolution interannual time series in the temperate North
426 Pacific. *ICES J. Mar. Sci.* **74**, 1906–1920 (2017).
- 427 **32.** Laffoley, D. & Baxter, J. M. *Ocean deoxygenation: Everyone’s problem-Causes, impacts, conse-*
428 *quences and solutions* (IUCN Gland, Switzerland, 2019).
- 429 **33.** Koslow, J. A., Goericke, R., Lara-Lopez, A. & Watson, W. Impact of declining intermediate-water
430 oxygen on deepwater fishes in the California Current. *Mar. Ecol. Prog. Ser.* **436**, 207–218 (2011).
- 431 **34.** Bianchi, D., Galbraith, E. D., Carozza, D. A., Mislan, K. & Stock, C. A. Intensification of open-ocean
432 oxygen depletion by vertically migrating animals. *Nat. Geosci.* **6**, 545–548 (2013).
- 433 **35.** Mais, K. F. Pelagic fish surveys in the California Current. *California Dep. Fish Game’s Fish Bull.*
434 (1974).
- 435 **36.** Laroche, J. L. & Richardson, S. Reproduction of northern anchovy, *Engraulis mordax*, off Oregon
436 and Washington. *Fish. Bull* **78**, 603–618 (1980).
- 437 **37.** Breitburg, D. L., Baumann, H., Sokolova, I. M. & Frieder, C. A. Multiple stressors–forces that
438 combine to worsen deoxygenation and its effects. In Laffoley, D. & Baxter, J. M. (eds.) *Ocean*
439 *deoxygenation: everyone’s problem. Causes, impacts, consequences and solutions* (International
440 Union for Conservation of Nature and Natural Resources, 2019).
- 441 **38.** Stevens, A. M. & Gobler, C. J. Interactive effects of acidification, hypoxia, and thermal stress on
442 growth, respiration, and survival of four North Atlantic bivalves. *Mar. Ecol. Prog. Ser.* **604**, 143–161
443 (2018).
- 444 **39.** Breitburg, D. L., Hondorp, D. W., Davias, L. A. & Diaz, R. J. Hypoxia, nitrogen, and fisheries:
445 integrating effects across local and global landscapes. *Annu. Rev. Mar. Sci.* **1**, 329–349 (2009).
- 446 **40.** de Mutsert, K. *et al.* Exploring effects of hypoxia on fish and fisheries in the northern Gulf of Mexico
447 using a dynamic spatially explicit ecosystem model. *Ecol. Model.* **331**, 142–150 (2016).
- 448 **41.** Nixon, S. W. & Buckley, B. A. “A strikingly rich zone”—nutrient enrichment and secondary
449 production in coastal marine ecosystems. *Estuaries* **25**, 782–796 (2002).

- 450 **42.** Marigomez, I., Múgica, M., Izagirre, U. & Sokolova, I. M. Chronic environmental stress enhances
451 tolerance to seasonal gradual warming in marine mussels. *PLoS One* **12**, e0174359 (2017).
- 452 **43.** Breitburg, D. Effects of hypoxia, and the balance between hypoxia and enrichment, on coastal fishes
453 and fisheries. *Estuaries* **25**, 767–781 (2002).
- 454 **44.** Keller, A. A. *et al.* Occurrence of demersal fishes in relation to near-bottom oxygen levels within the
455 California Current Large Marine Ecosystem. *Fish. Oceanogr.* **24**, 162–176 (2015).
- 456 **45.** Bertrand, A. *et al.* Oxygen: a fundamental property regulating pelagic ecosystem structure in the
457 coastal southeastern tropical Pacific. *PloS one* **6**, e29558 (2011).
- 458 **46.** Alegre, A. *et al.* Diet diversity of jack and chub mackerels and ecosystem changes in the northern
459 Humboldt Current system: A long-term study. *Prog. Oceanogr.* **137**, 299–313 (2015).
- 460 **47.** Bertrand, A. *et al.* 3-d habitat suitability of jack mackerel *Trachurus murphyi* in the Southeastern
461 Pacific, a comprehensive study. *Prog. Oceanogr.* **146**, 199–211 (2016).
- 462 **48.** Long, M., Ito, T. & Deutsch, C. Oxygen projections for the future. In Laffoley, D. & Baxter, J. M.
463 (eds.) *Ocean deoxygenation: everyone's problem. Causes, impacts, consequences and solutions*
464 (International Union for Conservation of Nature and Natural Resources, 2019).
- 465 **49.** Bograd, S. J. *et al.* Oxygen declines and the shoaling of the hypoxic boundary in the California
466 Current. *Geophys. Res. Lett.* **35** (2008).
- 467 **50.** Leinweber, A. & Gruber, N. Variability and trends of ocean acidification in the southern California
468 Current System: A time series from Santa Monica Bay. *J. Geophys. Res. Ocean.* **118**, 3622–3633
469 (2013).
- 470 **51.** Turi, G., Lachkar, Z., Gruber, N. & Münnich, M. Climatic modulation of recent trends in ocean
471 acidification in the California Current System. *Environ. Res. Lett.* **11**, 014007 (2016).
- 472 **52.** Bednaršek, N. *et al.* Synthesis of thresholds of ocean acidification impacts on decapods. *Front. Mar.*
473 *Sci.* **8**, 651102 (2021).
- 474 **53.** Bednaršek, N. *et al.* Synthesis of thresholds of ocean acidification impacts on echinoderms. *Front.*
475 *Mar. Sci.* **8**, 602601 (2021).
- 476 **54.** Lalli, C. M. & Gilmer, R. W. *Pelagic snails: The biology of holoplanktonic gastropod mollusks*
477 (Stanford University Press, 1989).
- 478 **55.** Hunt, B. *et al.* Pteropods in southern ocean ecosystems. *Prog. Oceanogr.* **78**, 193–221 (2008).
- 479 **56.** Armstrong, J. L. *et al.* Distribution, size, and interannual, seasonal and diel food habits of northern
480 Gulf of Alaska juvenile pink salmon, *Oncorhynchus gorbuscha*. *Deep. Sea Res. Part II: Top. Stud.*
481 *Oceanogr.* **52**, 247–265 (2005).
- 482 **57.** Aydin, K. Y., McFarlane, G. A., King, J. R., Megrey, B. A. & Myers, K. W. Linking oceanic food
483 webs to coastal production and growth rates of Pacific salmon (*Oncorhynchus spp.*), using models on
484 three scales. *Deep. Sea Res. Part II: Top. Stud. Oceanogr.* **52**, 757–780 (2005).
- 485 **58.** Karpenko, V. I., Volkov, A. & Koval, M. V. Diets of Pacific salmon in the Sea of Okhotsk, Bering Sea,
486 and northwest Pacific Ocean. *N. Pac. Anadr. Fish Comm. Bull* **4**, 105–116 (2007).
- 487 **59.** McLaughlin, K. *et al.* Core principles of the California Current Acidification Network: Linking
488 chemistry, physics, and ecological effects. *Oceanography* **28**, 160–169 (2015).

- 489 **60.** Hauri, C. *et al.* Spatiotemporal variability and long-term trends of ocean acidification in the California
490 Current System. *Biogeosciences* **10**, 193–216, DOI: [10.5194/bg-10-193-2013](https://doi.org/10.5194/bg-10-193-2013) (2013).
- 491 **61.** Shchepetkin, A. F. & McWilliams, J. C. The regional oceanic modeling system (ROMS): a split-
492 explicit, free-surface, topography-following-coordinate oceanic model. *Ocean. Model.* **9**, 347–404
493 (2005).
- 494 **62.** Moore, J. K., Doney, S. C. & Lindsay, K. Upper ocean ecosystem dynamics and iron cycling in a
495 global three-dimensional model. *Glob. Biogeochem. Cycles* **18** (2004).
- 496 **63.** Deutsch, C. *et al.* Biogeochemical variability in the California Current System. *Prog. Oceanogr.* **196**,
497 102565 (2021).
- 498 **64.** Renault, L. *et al.* Evaluation of high-resolution atmospheric and oceanic simulations of the California
499 Current System. *Prog. Oceanogr.* **195**, 102564 (2021).
- 500 **65.** Armstrong, R. A., Lee, C., Hedges, J. I., Honjo, S. & Wakeham, S. G. A new, mechanistic model for
501 organic carbon fluxes in the ocean based on the quantitative association of POC with ballast minerals.
502 *Deep. Sea Res. Part II: Top. Stud. Oceanogr.* **49**, 219–236 (2001).
- 503 **66.** Wanninkhof, R. Relationship between wind speed and gas exchange over the ocean. *J. Geophys. Res.*
504 *Ocean.* **97**, 7373–7382 (1992).
- 505 **67.** Kessouri, F. *et al.* Configuration and validation of an oceanic physical and biogeochemical model to
506 investigate coastal eutrophication in the Southern California Bight. *J. Adv. Model. Earth Syst.* **13**,
507 e2020MS002296 (2021).
- 508 **68.** Lewis, E., Wallace, D. & Allison, L. Program developed for CO₂ system calculations. Tech. Rep.,
509 Brookhaven National Lab., Dept. of Applied Science, Upton, NY (1998).
- 510 **69.** Sharp, J. D. *et al.* CO2SYSv3 for MATLAB, DOI: [10.5281/ZENODO.3950563](https://doi.org/10.5281/ZENODO.3950563) (2020).

511 **Acknowledgements**

512 This research was supported by NOAA grants NA15NOS4780186, NA18NOS4780174, and NA18NOS4780167
513 (Coastal Hypoxia Research Program), the California Ocean Protection Council grant C0100400NSF,
514 C0831014, and C0303000 (administered by California SeaGrant as R/OPCOAH-1), and the NSF grants
515 OCE-1419323 and OCE-1419450. This work used the Expanse system at the San Diego Supercom-
516 puter Center through allocation TG-OCE170017 from the Advanced Cyber Infrastructure Coordination
517 Ecosystem: Serves and Support (ACCESS) program, which is supported by National Science Foundation
518 grants 2138259, 2138286, 2138307, 2137603, and 2138296. Additional computational resources were
519 provided by the Hoffman2 computer cluster at the University of California Los Angeles, Institute for
520 Digital Research and Education (IDRE). Data and code needed to run the ROMS-BEC simulations are
521 available following the link: <https://github.com/UCLA-ROMS/Code>.

522 **Author contributions statement**

523 CAF conceived and designed the analysis, performed the analysis, and wrote the paper, FK performed
524 the simulations, conceived and designed the analysis, wrote the paper, MH performed the simulations
525 and conceived and designed the analysis, MS conceived and designed the analysis and wrote the paper,
526 DB conceived and designed the analysis and contributed analysis tools, JCW conceived and designed the
527 analysis and contributed analysis tools, CD conceived and designed the analysis and contributed analysis

528 tools, EH conceived and designed the analysis and contributed analysis tools. All authors reviewed the
529 manuscript.

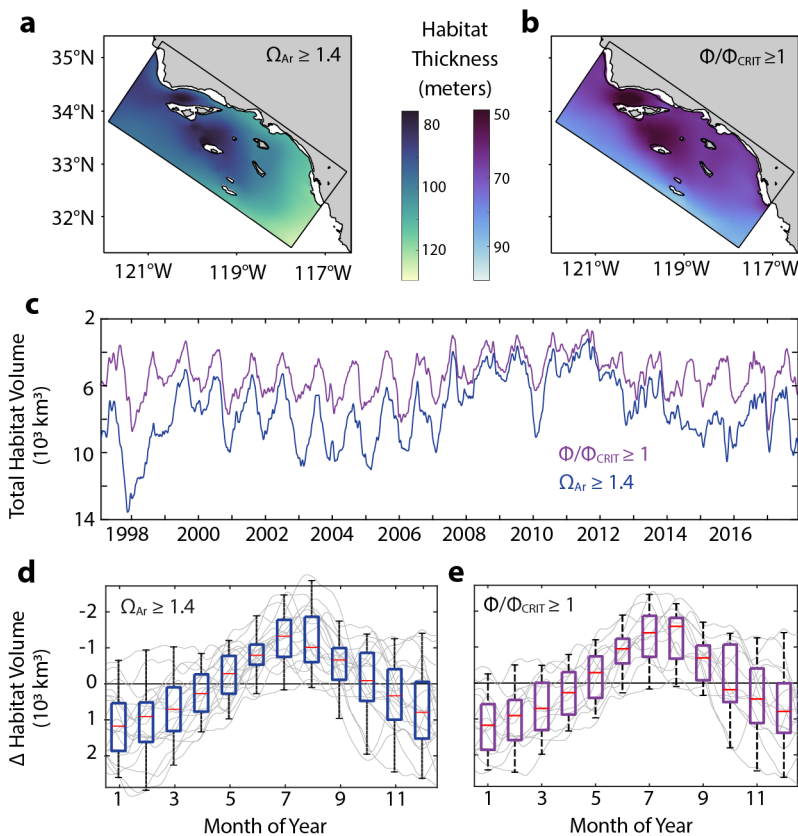


Figure 1. (a-b) Spatial distribution of mean habitat thickness (m) for each biological metric. Coastline and 200-m bathymetric contours (black) shown. Locations within the domain where habitat thickness interacts with seafloor not included. (c) Time-series of total habitat volume (10^3 km^3) summed across the model domain for $\Omega_{Ar} \geq 1.4$ (blue) and $\Phi/\Phi_{CRIT} \geq 1$ (purple). Model output is daily with a two-week running mean applied. (d-e) Seasonal trend in habitat volume for each biological metric. Each annual time-series is detrended with the annual mean (light grey). Box plots (median in red, 25th and 75th percentiles indicated by the bounded box, minimum and maximum as whiskers) for the average monthly values from the annually detrended time series shown ($n = 18$ years). Y-axes are oriented so that a decrease in habitat volume is upwards and an increase in habitat volume is downwards.

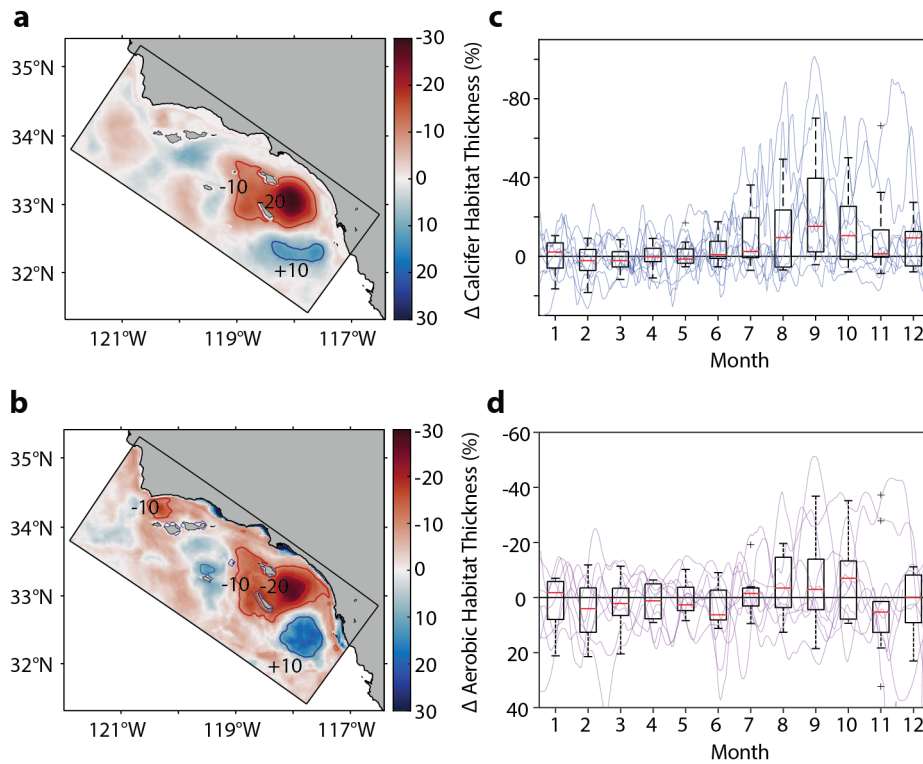


Figure 2. (a-b) Spatial distribution of the percent change in habitat thickness for $\Omega_{Ar} \geq 1.4$ and $\Phi/Phi_{CRIT} \geq 1.0$ between ANTH and CTRL (from average monthly output during time periods of maximum habitat loss, $n = 7$ events). Thin contours show regions undergoing -10 and +10% change in habitat thickness (red and blue, respectively). Thick red contour shows region experiencing more than -20% change in habitat thickness. (c-d) Seasonal trend of habitat compression within the region undergoing 20% loss in habitat thickness per metric (as contoured in A and B). Individual years (thin lines; $n = 9$) and box plots of mean monthly percent change in habitat thickness. Y-axes are oriented so that a compression in habitat thickness is upwards and an expansion in habitat thickness is downwards relative to zero.

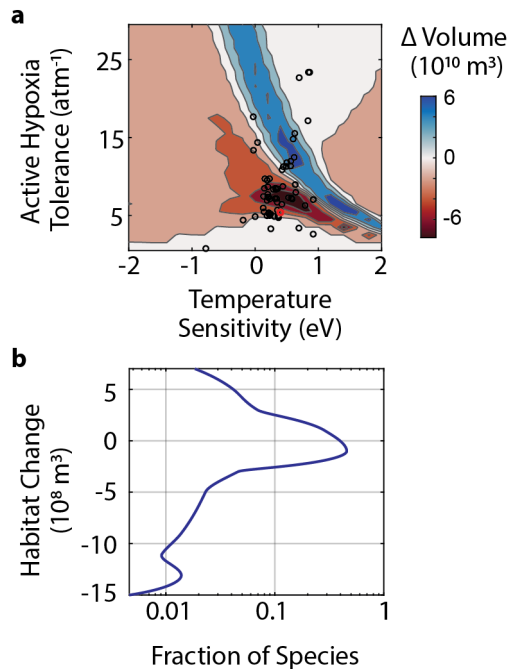


Figure 3. (a) Change in aerobic habitat from land-based nutrient inputs for varied marine ecophysiotypes. The range of Active Hypoxia Tolerance, A_o/Φ_{CRIT} , and temperature sensitivity, E_o , evaluated are based on a global species trait compilation; empirically derived species traits are marked with black circles, northern anchovy is marked with a red circle. Change in aerobic habitat volume assessed for the upper 200 m in the region undergoing 20% habitat compression (see Fig. 2 for region of focus) from months exhibiting maximum compression in the fall ($n = 7$) due to land-based nutrient inputs. (b) Fitted distribution of the fraction of species (log scale) undergoing trait-weighted volume changes in aerobic habitat. The change in habitat volume weighted by the probability distribution of the empirical traits³.

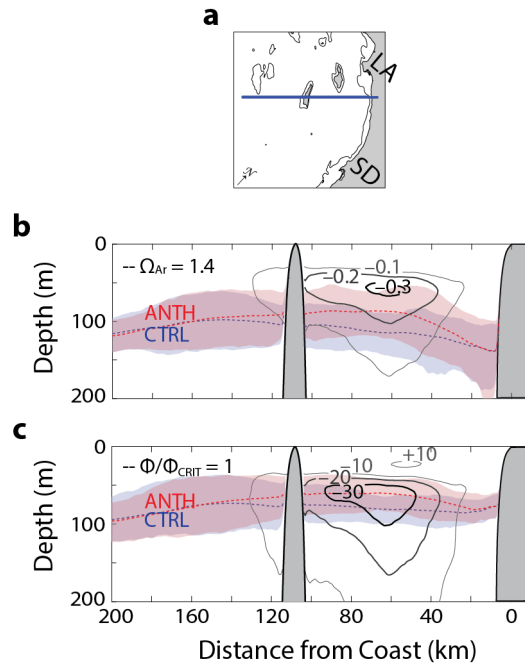


Figure 4. (a) Map of cross-section extending from the coast to 200 km offshore and intersected by San Nicolas Island. Coastline, Los Angeles (LA), San Diego (SD), and 200-m bathymetric contour shown. (b) Cross-section of mean absolute difference (contours) in Ω_{Ar} between the two simulations (ANTH-CTRL) from months exhibiting maximum compression in the fall ($n = 7$). Contour data overlaid with the mean depth of $\Omega_{Ar} = 1.4$ in the CTRL (blue dashed line) and ANTH (red dashed line) scenario along with 10th and 90th percentiles (shaded blue and red regions, respectively). (c) Same as in (b) but contours are the absolute difference in O_2 (mmol m^{-3}) between ANTH and CTRL overlaid with the mean lower depth limit of $\Phi/\Phi_{CRIT} = 1$.

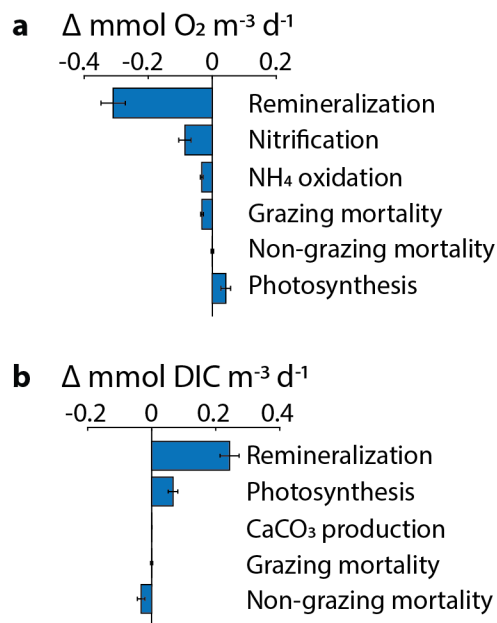


Figure 5. Absolute difference in the biogeochemical rate processes that contribute to the (a) O₂ and (b) dissolved inorganic C (DIC) cycles between the ANTH and CTRL scenarios. Data are monthly averages from within the region of 20% habitat compression (Fig. 2a) averaged from 70 to 140-m water depth (n = 104 months; mean ± 1 SE).

1 Supplemental Figures

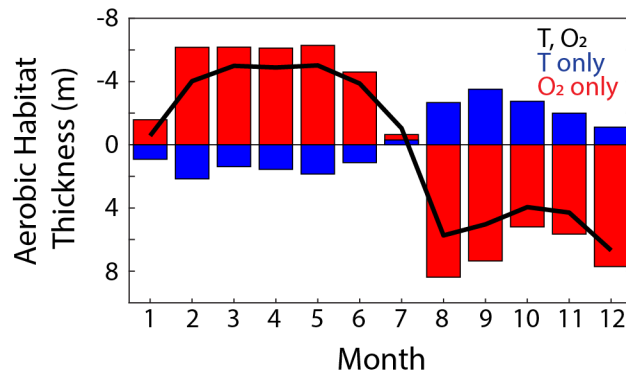


Figure S1. Mean monthly change in Habitat Thickness for $\Phi/\Phi_{CRIT} = 1$ parameterized for northern anchovy (*Engraulis mordax*; $A_O/\Phi_{CRIT} = 5.4 \text{ atm}^{-1}$, $E_O = 0.4 \text{ eV}$) calculated from model output 1997-2017 where both temperature and O₂ vary (thick black line), as well as change in habitat thickness due to temperature (blue bars) or O₂ (red bars) alone. Y-axis is oriented so that a decrease in habitat thickness is upwards.

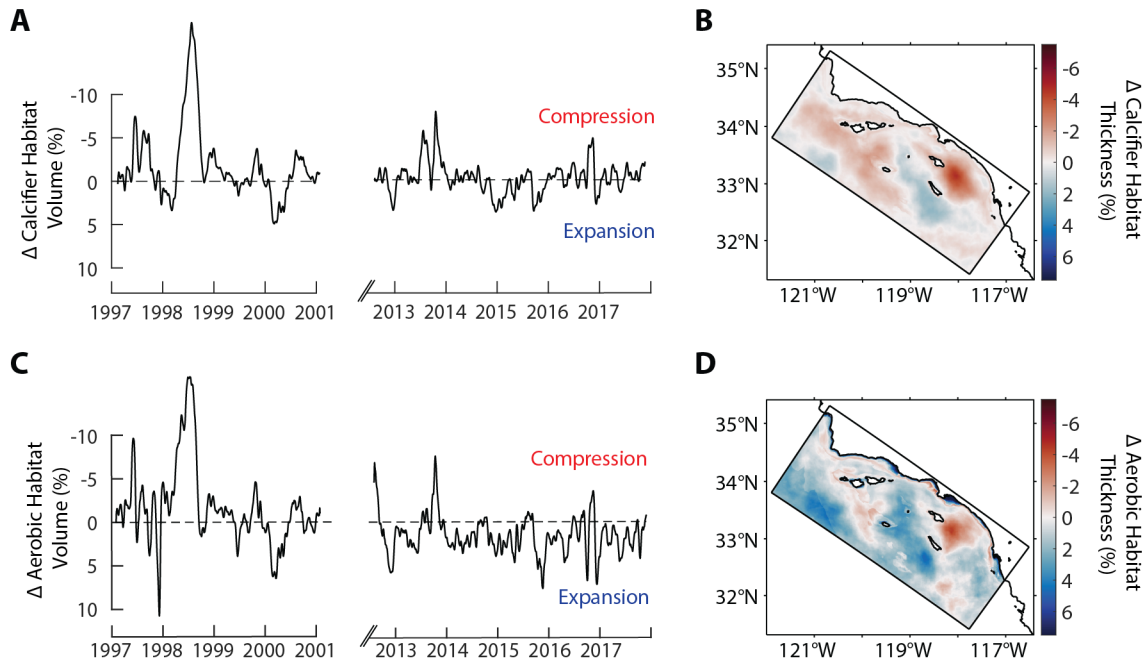


Figure S2. (A,C) Time-series of the percent change between the ANTH and CTRL simulations in total habitat volume averaged across the model domain for $\Omega_{Ar} \geq 1.4$ and $\Phi/\Phi_{CRIT} \geq 1$. Model output is daily with a two-week running mean. (B,D) Spatial distribution of the percent change in habitat volume for $\Omega_{Ar} \geq 1.4$ and $\Phi/\Phi_{CRIT} \geq 1$ averaged across the entire time period of simulations (1998 removed as an outlier year). Coastline and model domain (black outer box) shown. Negative versus positive values indicate time periods or regions undergoing habitat compression versus expansion, respectively, in the ANTH scenario relative to the CTRL scenario. Y-axes are oriented so that a decrease in habitat volume or thickness is upwards.

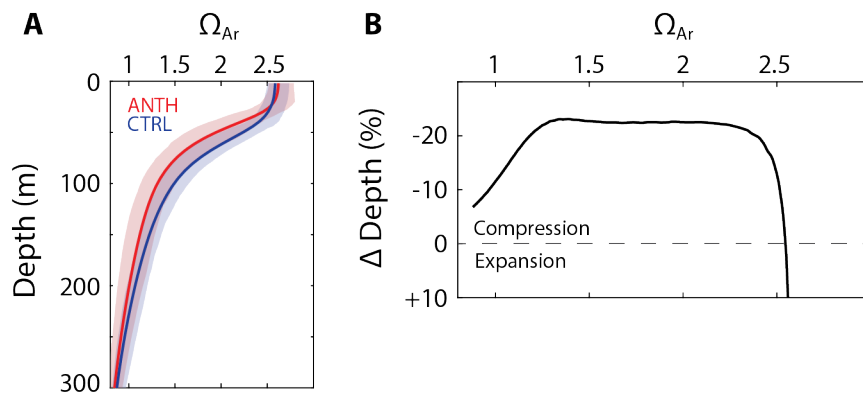


Figure S3. Sensitivity analysis for a range of values of Ω_{Ar} considered suboptimal for calcifiers. (A) Mean aragonite saturation state (Ω_{Ar}) as a function of depth for ANTH (red) and CTRL (blue). Shaded region represents 10th and 90th percentile of conditions. Profile data from Fig. 4 focused on region of maximum impact, averaged 60 – 80 km from shore. (B) Percent change in depth at which a given value of Ω_{Ar} occurs between ANTH and CTRL. Negative values represent a shoaling (compression) of Ω_{Ar} conditions in the ANTH simulation relative to CTRL.

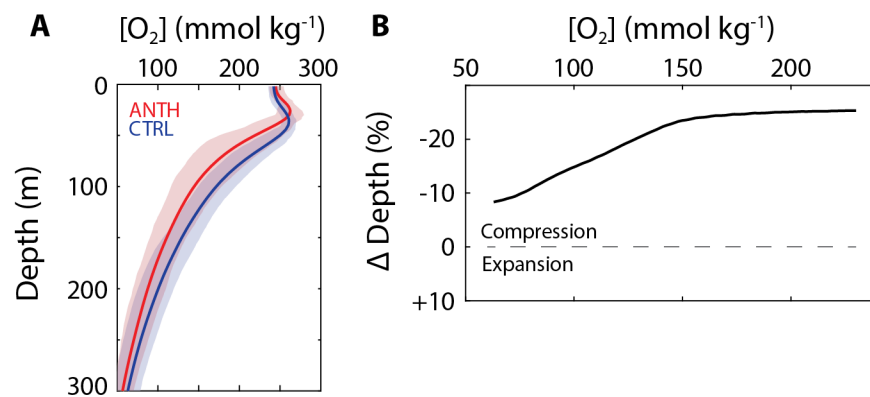


Figure S4. Sensitivity analysis of species parameterization of aerobic habitat. (A) Mean $[O_2]$ as a function of depth for ANTH (red) and CTRL (blue). Shaded region represents 10th and 90th percentile of conditions. Profile data from Fig. 4 focused on region of maximum impact, averaged from 60 – 80 km from the coast. (B) Percent change in depth at which a given value of O_2 occurs between ANTH and CTRL. Negative values represent a shoaling (compression) of $[O_2]$ in the ANTH simulation relative to CTRL. Surface conditions (with increased $[O_2]$ under the ANTH scenario) not included.

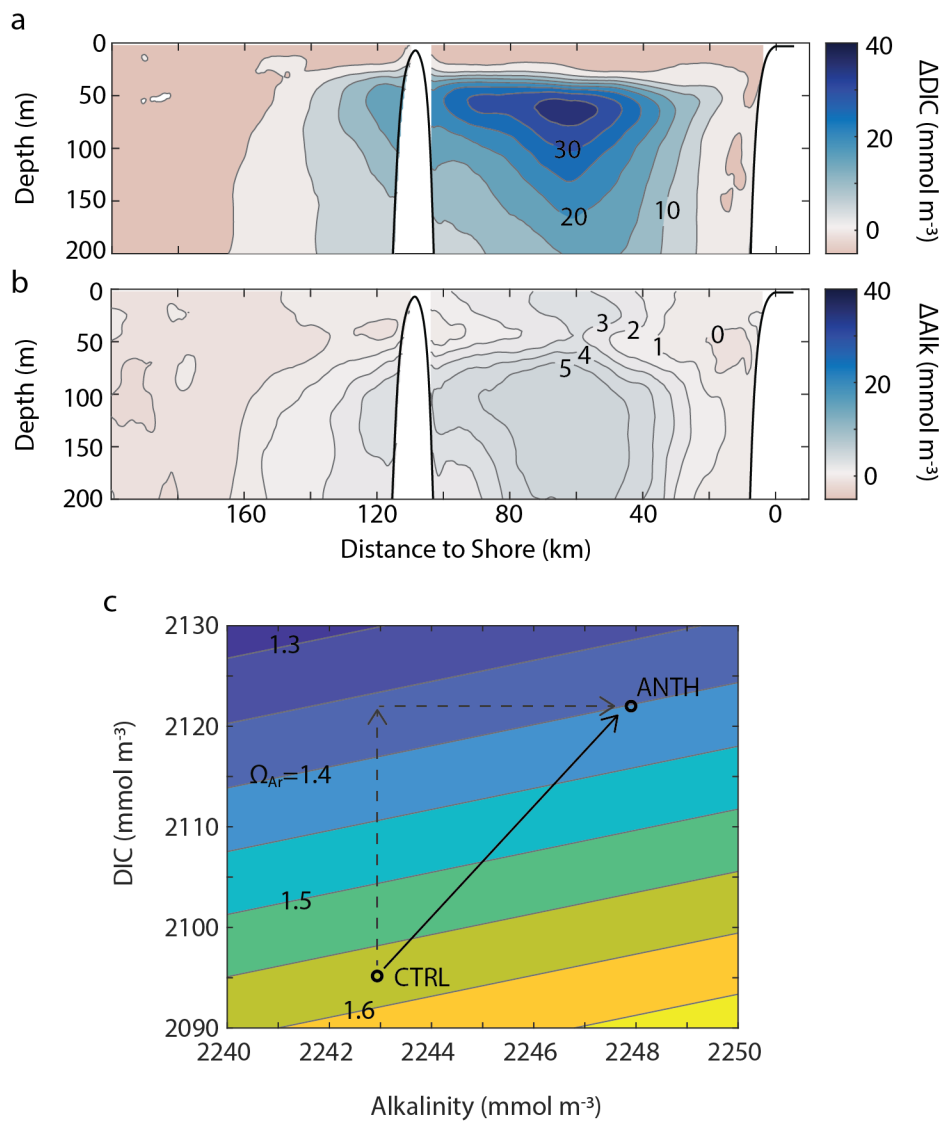


Figure S5. (A-B) Cross-section of mean absolute difference (contours) in dissolved inorganic carbon (DIC) and alkalinity (Alk) between the two scenarios (ANTH-CTRL) from months exhibiting maximum compression in the fall ($n = 7$). Cross-section plotted as shown in Fig. 4A. (C) Mean alkalinity and DIC in the core of habitat compression (60 – 80 km from the coast and between 30 and 150 m water depth) in the CTRL and ANTH simulation (open circles) along with contours for calculated $\Omega_{Ar,T}$.